Chapter 9. Beam Loss and Collimation

M. Church, A. Drozhdin, O. Krivosheev, N. Mokhov

9.1. Introduction

A very high beam power of ~1.2 MW (4 MW in Phase II) implies serious constraints on beam losses in the machine [1, 2]. As will be shown below, the main concerns are hands-on maintenance and ground-water activation. Only with a very efficient beam collimation system [3] can one reduce uncontrolled beam losses in the machine to an allowable level. Massive local shielding is needed around the collimators. The entire complex must be well shielded to allow a non-controlled access to the outside surfaces under normal operation and accidental beam loss.

There are three 63.921 meter long straight sections in the Proton Driver lattice. Thr first of them, P20, together with 17 m of the preceding arc, called below "utility section", is used for beam injection and collimation (Fig. 9.1). The β-functions and dispersion in this region and along the ring are shown in Fig. 9.1 and Fig. 9.2.

In this study, a multi-turn particle tracking in the accelerator defined by all lattice components with their realistic strengths and aperture restrictions, and halo interactions with the collimators is done with the STRUCT [4] code. Protons lost on the machine components are stored in the files for the next step of calculations with the MARS [5] code. Full-scale Monte Carlo hadronic and electromagnetic shower simulations in the lattice elements, shielding, tunnel and surrounding dirt with realistic geometry and materials and magnetic field are done with MARS14. This shapter summarizes the results on tolerable beam loss and on a proposed beam collimation system design.

9.2. Deduction of Tolerable Beam Loss

To determine tolerable beam loss in the arcs, MARS14 simulations are done in the arc cells. A detailed lattice description with dipoles, quadrupoles and long bare beam pipes has been implemented into a 3-D model with corresponding materials and magnetic field distributions (see Figs. 9.3 and 9.4). A 16-GeV proton beam is assumed to be lost on a beam pipe at a grazing angle of 1 mrad inward. It is distrubuted uniformly along the arc lattice. Results are normalized per 1 W/m beam loss rate, that corresponds to 3.9×10^8 p/(m·sec). In this simplified model, a round 2-m radius tunnel with a 0.4-m concrete wall followed by wet dirt is assumed with the beam line in the center. Dose accumulated in the hottest spots of the coils, residual dose rates on the outer surface of the lattice elements after 30 days of irradiation and 1 day of cooling, and ground-water activation and dose attenuation in the surrounding dirt are calculated. Regulatory requirements of Section 10.2 are taken as the limits to be met.

Maximum residual dose rates calculated for the arc elements at 1 W/m uniform beam loss are shown in the third column of Table 9.1. The table gives also the peak dose ac-

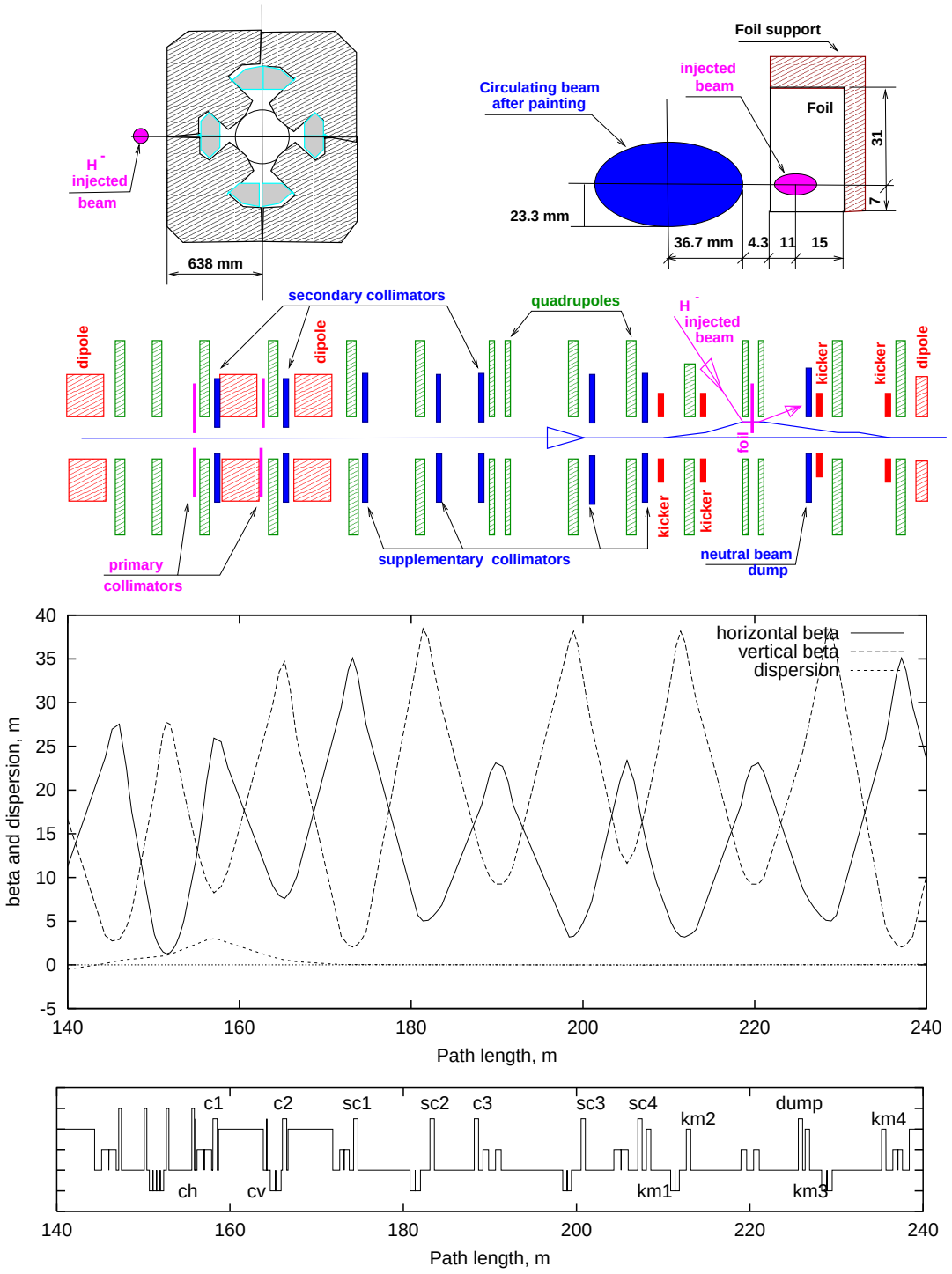

Figure 9.1. Beam collimation and beam painting systems (top) and beta functions and dispersion in the utility section (bottom).

cumulated in the coils and the parameter C_{tot} calculated according to Eq. (10.2). The last column gives corresponding beam loss rates calculated to meet the limits of Section 10.2: P_γ=100 mrem/hr, D=20 Mrad/yr and C_{tot}=1.

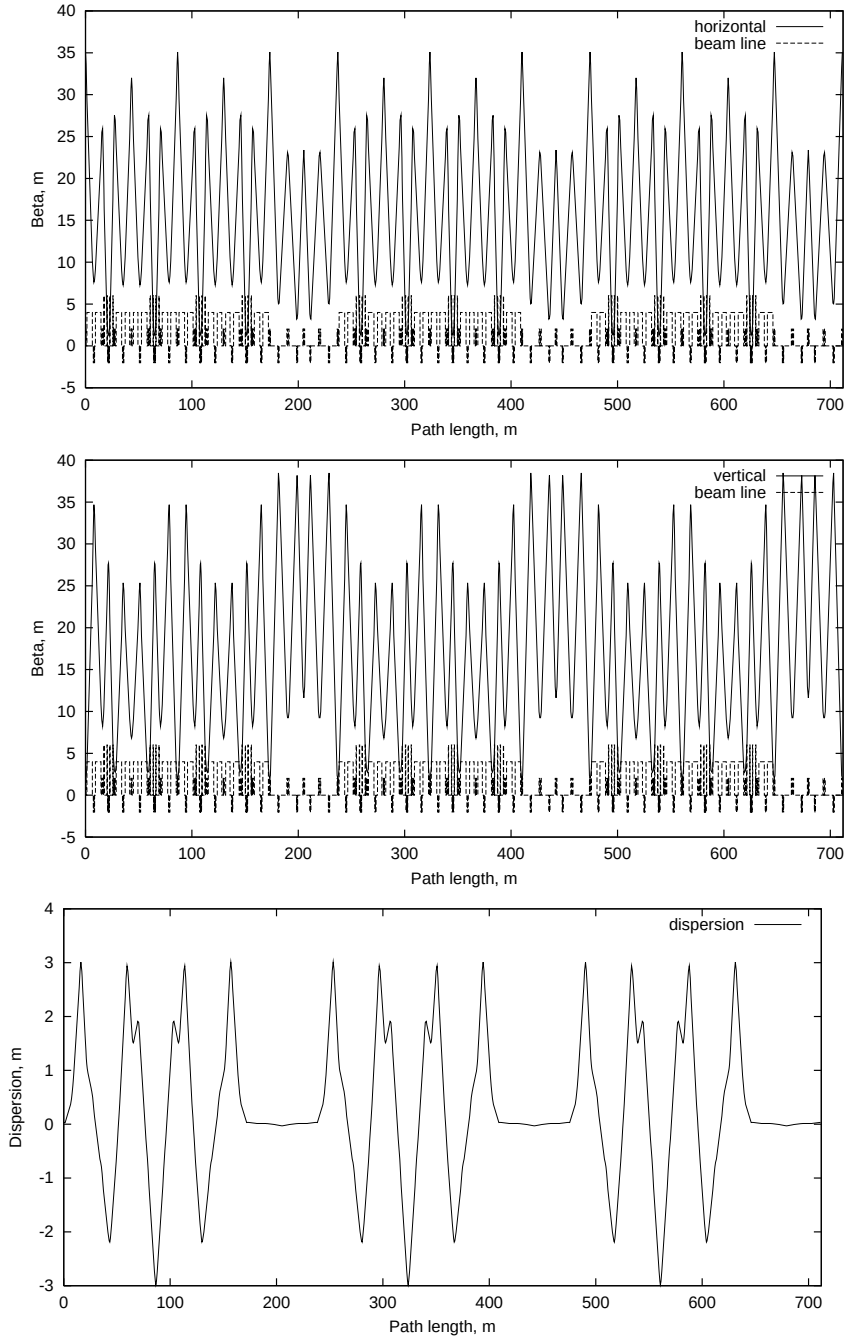

Figure 9.2. Proton Driver beta functions and dispersion.

The dose near the bare beam pipes exceeds the design goal for hot regions of 100 mrem/hr; it is noticeably lower near the magnets due to significant absorption of soft photons in the dipole and quadrupole materials. One sees that hands-on maintenance is a serious issue with about 3 W/m as a tolerable maximum beam loss rate in the lattice elements, except for the long bare beam pipes where one should decrease the loss rate to 0.25 W/m to reduce the dose to 100 mrem/hr. One needs further reduction to bring the dose down to a good practice value

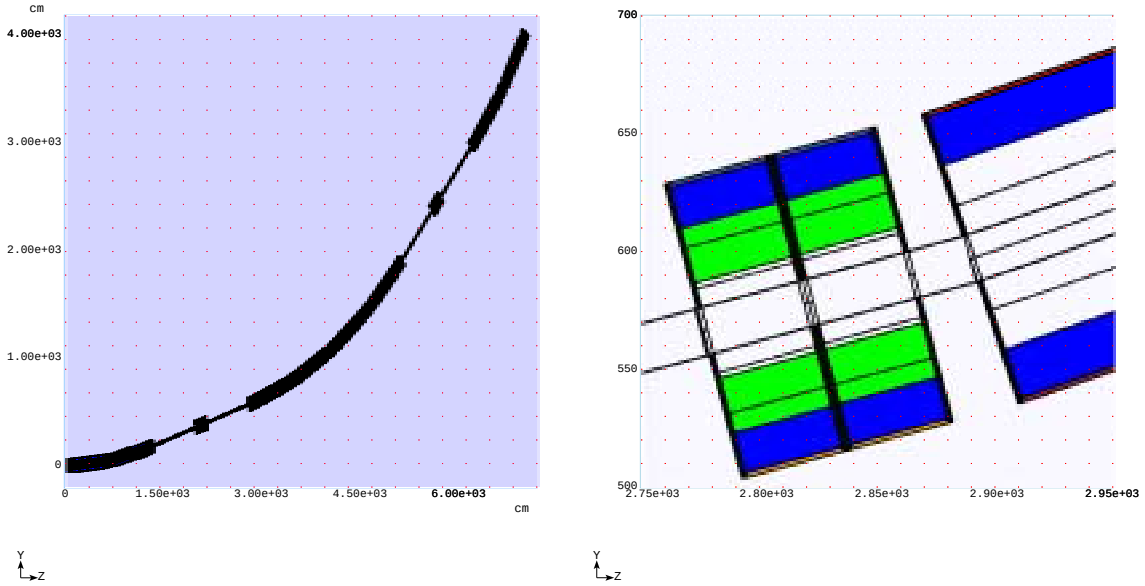

Figure 9.3. MARS model of a Proton Driver arc cell.

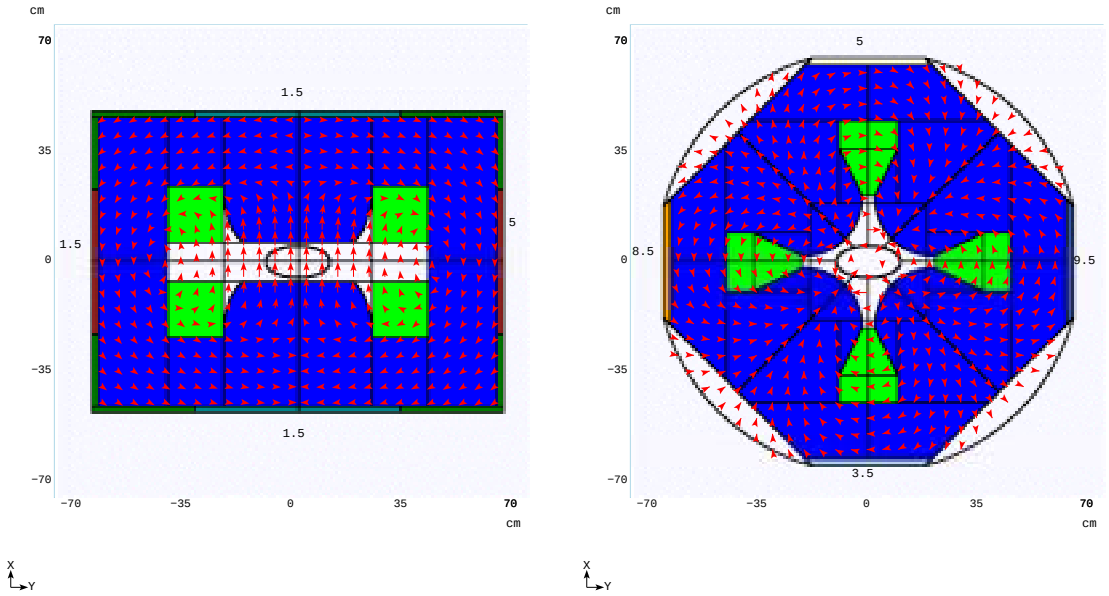

Figure 9.4. MARS model of arc dipole (left) and quadrupole (right).

of about 10-20 mrem/hr. Alternatively, one can think of providing simple shielding around the bare beam pipes. For ground-water activation C_{tot}=0.975 immediately outside the 40-cm tunnel wall (see Eq. (10.2)), that allows 1.03 W/m beam loss rate. The peak accumulated dose in the coils is about 2 Mrad/yr at 1 W/m beam loss rate which is acceptable with use of appropriate materials for insulation.

Table 9.1. Peak residual dose rate P_γ on 16 GeV lattice elements, accumulated dose D in dipole and quadrupole coils, ground-water activation parameter C_{tot} and allowable beam loss rate.

Value	Element	Peak at 1 W/m	Allowable loss (W/m)
P_γ (mrem/hr)	Long pipe	400	0.25
	Quad side	9.4	10.6
	Quad flange	34	2.94
	Dipole side	5	20
	Dipole flange	20	5
D (Mrad/yr)	Coil	2	10
C_{tot}	Ground water	0.98	1.03

9.3. Goals and Principles of Collimation

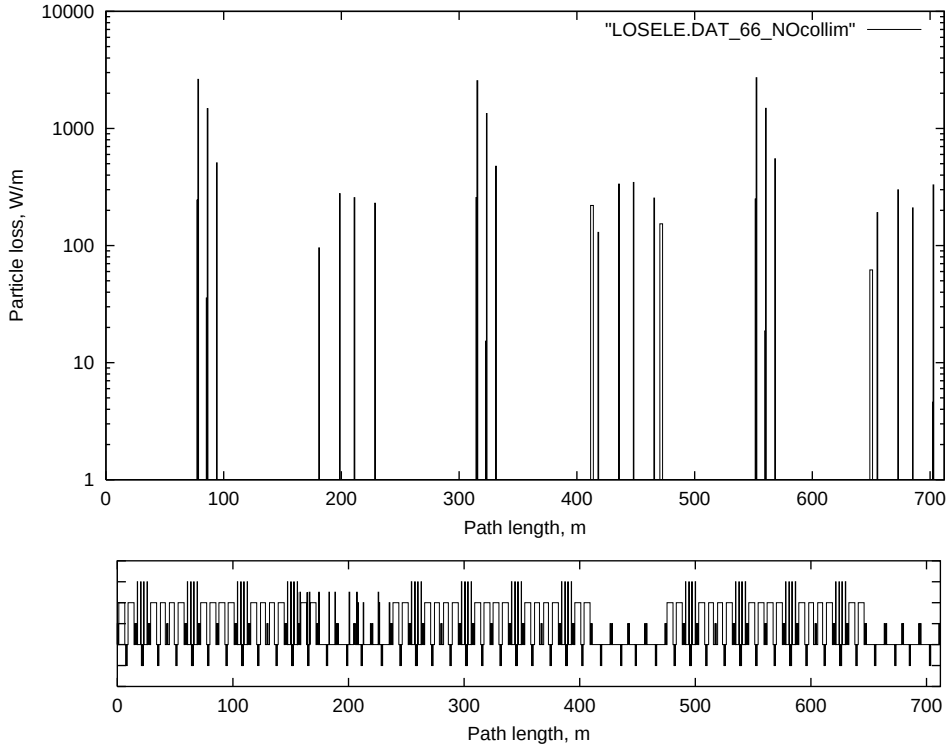

Figure 9.5. Beam loss distribution without collimators at 1% loss of intensity.

The beam power at the top accelerator energy is 1.152 MW. Assuming that 1% of the beam is lost at steady growth of the beam size and momentum spread, this amounts to 11.52 kW of beam loss distributed around the ring (Fig. 9.5) with a peak loss of up to 2 kW/m on several quadrupoles. This level is 2000 times higher than that which can be accepted in the arcs. The purpose of the beam halo cleaning system is to localize proton losses in a specially

shielded short section. This reduces irradiation of the rest of the machine to the acceptable levels described in the previous section.

A two-stage collimation is proposed [3, 8] with a set of primary and secondary collimators. At normal operating conditions, a circulating beam size grows slowly with a small step size per turn. A corresponding proton impact parameter on a collimator would be of the order of few μm. A thin primary collimator, introduced into the lattice as a limiting aperture, increases proton amplitude as a result of multiple Coulomb scattering and thus results in drastic increase of impact parameter on the downstream secondary collimators. This results in a significant reduction of the out-scattered proton yield and total beam loss in the accelerator, decreases collimator jaw overheating and mitigates requirements on the collimator alignment [3, 8].

9.4. Collimation System Design Analysis

9.4.1. Collimation at injection and top energy

A two-stage beam collimation system is designed using the available spaces in the utility section. It consists of horizontal and vertical primary collimators CH, CV, secondary collimators C1-C3, and supplementary collimators SC1-SC4 (Fig. 9.1 and Table 9.2).

Table 9.2. β-functions, dispersion and phase advance between the primary and secondary collimators.

Collimator	β-function (m)		Dispersion (m)	Phase advance between primary and secondary collimators (deg)	
	horizontal	vertical		horizontal	vertical
Horizontal primary CH	19.7	10.0	2.8	0	-
Secondary C1	24.8	10.4	2.8	5	-
Vertical primary CV	8.4	31.7	0.8	-	0
Secondary C2	9.6	30.7	0.4	45	4
Supplementary SC1	30.3	3.8	0.0	69	100
Supplementary SC2	6.9	31.5	0.0	125	140
Secondary C3	20.0	12.4	0.0	152	156
Supplementary SC3	7.3	30.0	0.0	253	198
Supplementary SC4	15.7	19.1	0.0	279	221
Neutral beam dump	7.7	26.5	0.0	411	283

Secondary collimators need to be placed at phase advances which are optimal to intercept most of particles out-scattered from the primary collimators during the first turn after the halo interaction with the primary collimator. Transverse phase space at the collimators is shown in Fig. 9.6. The optimal phase advances are around $k \cdot \pi \pm 30^o$. Phase advances between the primary and secondary collimators are presented in Table 9.2. The horizontal and vertical secondary collimators C1 and C2 and collimator C3 with jaws in both horizontal and

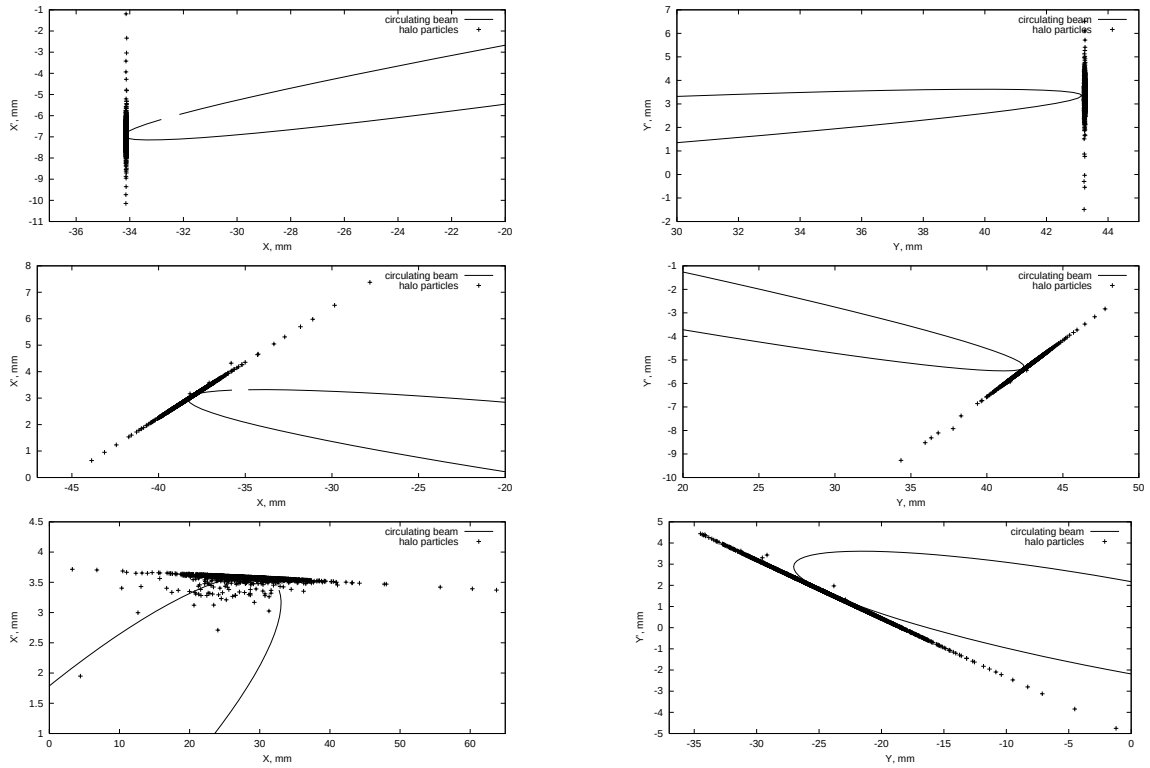

Figure 9.6. Horizontal (left) and vertical (right) phase space at the primary collimators (top), secondary collimators C1 and C2 (middle), and C3 (bottom).

vertical planes have good phase advances with respect to the primary collimator. The horizontal and vertical primary collimators are placed at the edge of the beam after painting. The beam loss distribution at the top accelerator energy with three secondary collimators located at 2 mm from the beam edge is shown in Fig. 9.7. The jaws of the secondary collimators should be made of stainless steel about 3 cm thick and 0.5 m long. It is assumed in calculations that 0.66% of the beam is lost on the horizontal primary collimator (half for off-momentum protons with $\Delta p/p = \pm 0.002$ and half for on-momentum protons) and 0.33% is lost on the vertical primary collimator.

The right side of Fig. 9.7 shows details of beam loss in the collimation region. Secondary collimators generate out-scattered particles lost later in the lattice. One can reduce this component with a *3-stage collimation system* positioning several *main* secondary collimators close to the beam to deal with protons scattered in the primary collimator and several *supplementary* collimators farther from the beam to catch particles out-scattered from the main secondary collimators. Beam loss distributions with 3 and 5 supplementary collimators 0.5 m long located at 5 mm from the beam edge are shown in the middle and bottom of Fig. 9.7. One can see significant reduction of beam loss rates with the proposed system. Table 9.3 summarizes results of this optimization.

The thickness and material of primary collimators affect the out-scattered proton angular distribution and nuclear interaction rate. Such a thin scatterer should give a considerable an-

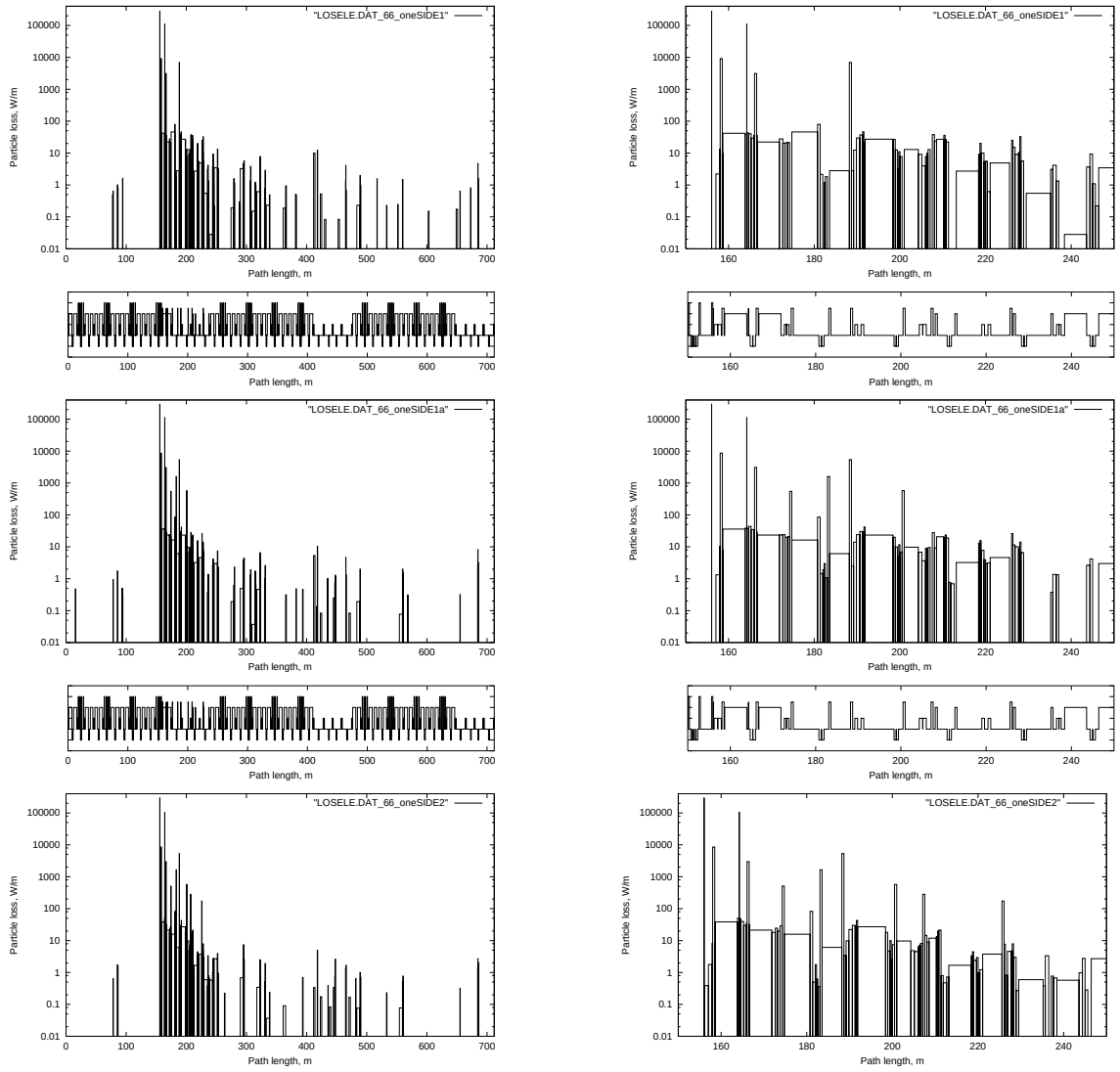

Figure 9.7. Beam loss at the top accelerator energy with secondary collimators at a 2 mm offset with respect to the primary ones (top), with three additional supplementary collimators SC1-SC3 at 5 mm offset (middle) and with five supplementary collimators (bottom).

gular kick to the halo particles, but their amplitude should remain smaller than the machine aperture on their way to the secondary collimators. Calculated beam losses are presented in Table 9.4 for 0.5, 1 and 1.5 mm thick tungsten collimators. A 1 mm collimator provides minimal loss rate in the ring.

The β-function varies along the length of a secondary collimator, therefore the collimator jaws are assumed to be aligned to follow the beam envelope after the painting. Longer secondary collimators reduce the punchthrough probability. We found that at 16 GeV the minimal length is 0.3 m of steel, with the optimum of about 0.5 m (see Table 9.5). The results shown are for 1 mm thick tungsten primary collimators and for secondary and sup-

Table 9.3. Beam loss in the Proton Driver. Total losses at injection (E_{kin} = 0.4 GeV) are assumed to be ∼2.88 kW, at the top energy (E_{kin} = 16 GeV) - ∼11.52 kW.

	Beam loss		
Collimation system	Utility section	Rest of the ring	Peak loss rate in the ring
	kW	kW	W/m
AT THE TOP ENERGY			
No collimators	0.470	11.050	2700
two-side collimators			
three secondary at 2 mm five supplementary at 5 mm	11.432	0.089	9.0
one-side collimators			
three secondary at 2 mm	11.375	0.146	13.2
three secondary at 2 mm three supplementary at 5 mm	11.422	0.098	10.4
three secondary at 2, 2 and 3 mm five supplementary at 5 mm	11.449	0.071	6.7
three supplementary - one-side, two others two-side			
three secondary at 1, 1 and 2 mm five supplementary at 3 mm	11.476	0.044	4.9
three secondary at 2, 2 and 3 mm five supplementary at 5 mm	11.462	0.059	6.6
three secondary at 3, 3 and 4 mm five supplementary at 7 mm	11.449	0.071	6.8
with bump three secondary at 2, 2 and 3 mm five supplementary at 5 mm	11.487	0.033	4.7
AT INJECTION three supplementary - one-side, two others two-side			
three secondary at 2, 2 and 3 mm five supplementary at 5 mm	2.879	0.001	0.2
at RF capture loss three secondary at 2, 2 and 3 mm five supplementary at 5 mm	2.877	0.003	1.0

Table 9.4. Beam loss as a function of tungsten primary collimators thickness.

Thickness	Utility section	Rest of the ring	Peak loss rate in the ring
mm	kW	kW	W/m
0.7	11.445	0.075	7.9
1.0	11.461	0.059	6.6
1.5	11.453	0.067	6.4

plementary collimators position as above.

Table 9.5. Beam loss as a function of steel secondary collimators length.

Length	Utility section	Rest of the ring	Peak loss rate in the ring
m	kW	kW	W/m
0.3	11.393	0.127	14.7
0.5	11.461	0.059	6.6
0.8	11.499	0.021	3.8

With the proposed system, ∼99% of the beam halo energy is intercepted in the 80-m long utility section. About 1% is lost in the rest of the machine along 630 m length with a mean rate of 0.12 W/m. At several locations the beam loss is noticeably higher (∼7 W/m), exceeding the tolerable rates of 0.6 W/m. The above hot locations should be taken care of via local shielding if necessary. Beam loss rates in the collimation system section itself are very high implying a special shielding design (see Section 10). Collimators, magnets and other equipment of the utility section require special cooling as well as fast disconnects and remote control.

9.4.2. Collimation during the accelerator cycle

It is assumed that 10% of the intensity is intercepted at injection, and 1% at the top energy. A practicality in a rapid cycling proton synchrotron dictates a stationary collimator approach with collimator jaws in a fixed position with respect to the beam orbit during the entire cycle. In the optimal configuration described in the previous section, the primary collimators are positioned at the edge of the beam after beam painting in the horizontal and vertical planes with the secondary and supplementary collimators farther from the beam.

In an ideal case, the edge of the circulating beam should be kept at these conditions during the total cycle. This requires rather complicated horizontal and vertical bumps, created by at least ten fast magnets for each direction. To simplify the system, we propose to keep the beam at the edge of the primary collimators and close to the first secondary collimators using only three fast magnets for each direction. Most of the particles scattered out of the primary collimators are intercepted now by these secondary collimators, with other collimators intercepting the larger amplitude and off-momentum protons. Such a scheme allows to localize a majority of the beam loss in a short 35-m long region with the maximum rate of (120-50) W/m in two dipoles immediately downstream of collimator C1 and C2, and to reduce the average loss in the ring from 0.12 W/m to 0.05 W/m. Corresponding beam loss distributions at injection and at the top energy are shown in Fig. 9.8 and in Table 9.3.

9.4.3. Beam collimation at RF capture

The efficiency of the collimation system depends on the impact parameter at the primary collimators. Particle coordinate step size at the collimator is defined by the particle mo-

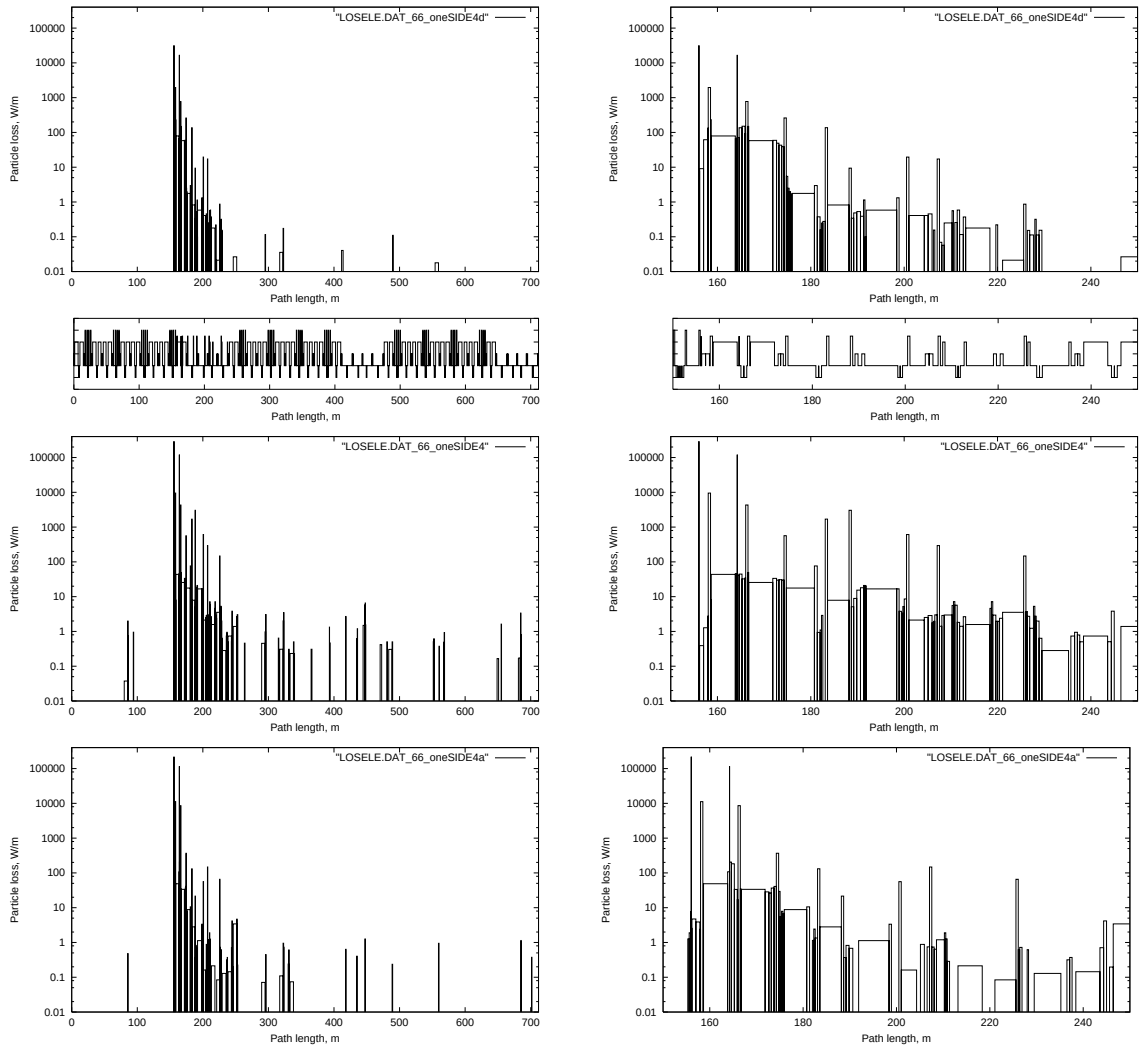

Figure 9.8. Beam loss at injection (top) and at the top energy (middle) without bump. Beam loss at the top energy with horizontal and vertical bump for keeping edge of the beam near the primary and first secondary collimators during the total cycle (bottom). It is assumed that 10% of intensity is lost at injection and 1% at the top energy.

mentum deviation with time and by the rate of particle betatron amplitude growth caused by the possible approach to betatron resonances, beam-gas interactions and other reasons. The first effect may significantly increase an impact parameter at the collimator if particles are lost off the separatrix at injection. The reason for simulations described here is to define the rate of particle energy evolution during this process and conditions for particles loss at the primary collimator, but not to investigate the RF capture itself. Because of this we did these simulations with assumptions which simplify calculations. For simulations of particle loss during RF capture the initial protons were placed in the vicinity of an unstable point. Synchro-betatron oscillations at the RF capture were simulated in the STRUCT code with longitudinal dynamics described by the difference equations for proton motion with respect to the synchronous particle [9]:

$$\varphi_i = \varphi_{i-1} - 2\pi \cdot f_{RF} \cdot f_{rev}^{-1} \left[\alpha - \frac{1}{\gamma^2}\right] \frac{\Delta E}{\beta^2 \cdot E_s}, \tag{9.1}$$

$$E_{exit} = E_{entrance} + \frac{e \cdot U}{1000} \left[\sin(\varphi_I) - \sin(\varphi_s)\right], \tag{9.2}$$

where

φ_I is the RF phase at particle pass through the cavity (radian);

φ_{I-1} is the RF phase at the previous turn (radian);

φ_s is the synchronous phase at the beginning of acceleration (radian);

E_s =1338.3 MeV is the synchronous energy;

f_{RF} = 37.864$\times 10^6$ Hz is the RF frequency at the beginning of acceleration for the first stage of project;

f_{RF} = 5.4091$\times 10^6$ Hz is the RF frequency at the beginning of acceleration for the second stage of project;

f_{rev} = 0.3$\times 10^6$ Hz is the revolution frequency at injection;

α = -0.000744 is the momentum compaction factor; we neglect the dependence of α on proton momentum;

$\gamma = E_s/(m_o \times c^2)$ = 1.4263 is the γ factor;

U is the RF voltage at the beginning of injection.

The RF voltage, synchronous phase φ_s and longitudinal phase space at the beginning of acceleration are shown in Fig. 9.9. The maximum energy deviation from the synchronous energy in the bucket at injection is ΔE=1 MeV for f_{RF}=37.86 MHz and ΔE=2.5 MeV for f_{RF}=5.41 MHz. Fig. 9.10 shows evolution of the longitudinal phase space of particles lost from the separatrix during this process. The duration of synchrotron oscillation for particles lost from the separatrix is about 2 turns for f_{RF}=37.86 MHz and 20 turns for f_{RF}=5.41 MHz. The impact parameter at the primary collimator is defined by the particle coordinate growth during 3-5 turns. During this time, particle momentum may change by several hundred keV (Fig. 9.10) affecting impact parameter increase at the primary collimator to 1-2 mm. Corresponding transverse distributions at the primary collimator and momentum spectrum of the lost protons are shown in Fig. 9.11. Most of halo protons on the primary collimator have $\Delta p/p \leq 1\%$. Beam losses at injection in the utility section and in the entire ring are presented in Fig. 9.12; for the beam size growing slowly, with impact parameter of 20 μm, and for beam loss at RF capture.

9.4.4. Crystal collimation

In this section we explore the possibility to use a crystal instead of an amorphous primary collimator, studied earlier for the Tevatron beam scraping system [10]. To evaluate the efficiency for such a collimation system, realistic simulations have been performed with CATCH

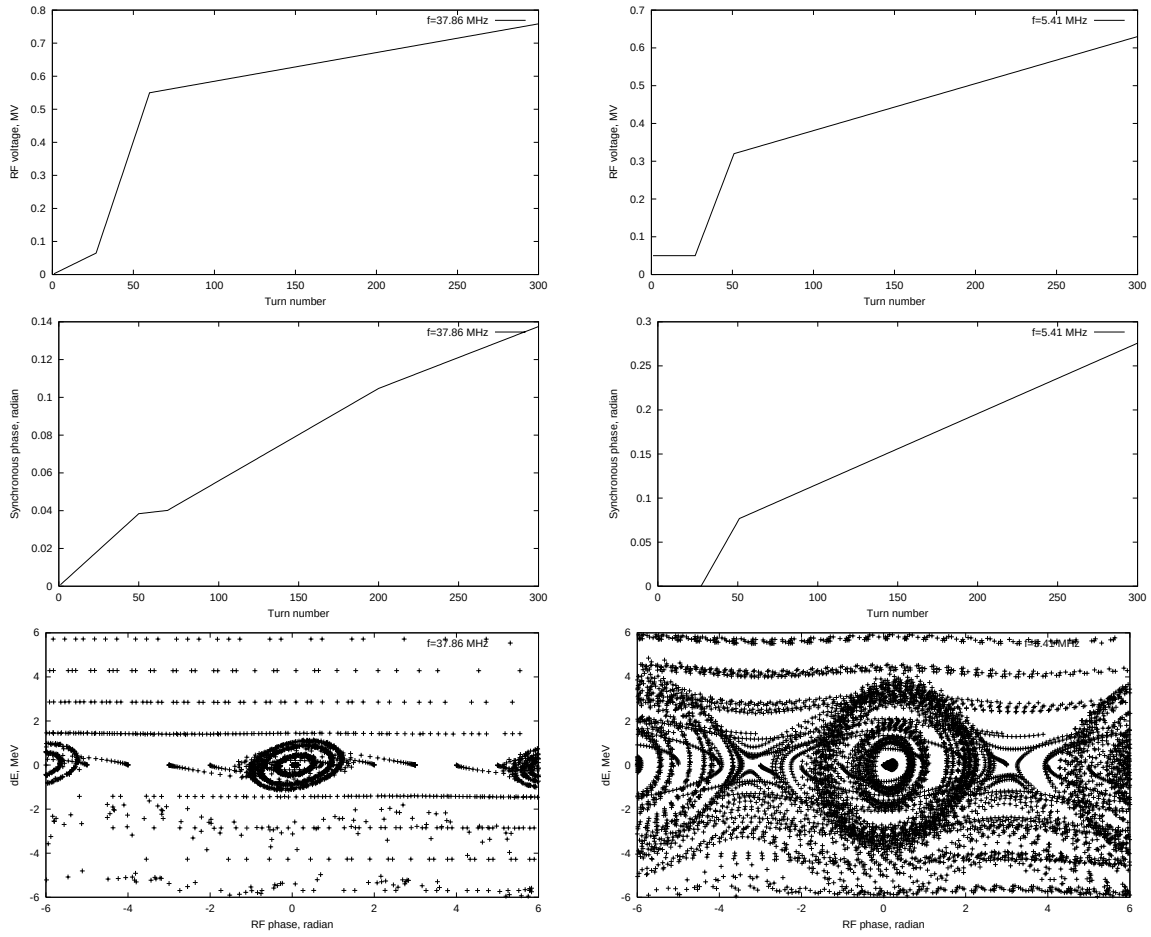

Figure 9.9. RF voltage (top), φ_s (middle) and longitudinal phase space (bottom) at RF capture for the Stage 1 f_{RF} = 37.86 MHz (left) and for Stage 2 f_{RF} = 5.41 MHz (right).

[11] linked to the STRUCT code. Crystal channeling is simulated in CATCH as described in "Crystal Channeling and its Application at High Energy Accelerators" Ref. [12]. Interactions with a crystal amorphous layer and all other near-beam interactions and tracking are performed with STRUCT.

An optimal Si(110) crystal radius is estimated as R (mm)$\approx 30 \times p\beta$, where p is proton momentum (GeV/c) and β is its velocity relative to the speed of light. Corresponding crystal length needed to deflect a proton by an angle θ is L = Rθ. A 3-mm silicon crystal deflects 16-GeV protons by 5.9 mrad. A crystal critical angle, estimated as α(mrad)$\approx 0.15/\sqrt{p\beta}$, is 0.18 mrad at injection and 0.036 mrad at 16 GeV. For channeling to occur, these angles should be larger than the beam divergence. Another parameter, especially important at low energies, is the crystal dechanneling length L_{dechan}(mm) $\approx p\beta$, that is 0.7 mm at 400 MeV and 17 mm at 16 GeV. In a rapid cycling machine the same crystal should be used both at injection and at the top energy. It is clear that the requirement L ¡ L_{dechan} is violated at injection.

In this study an attempt was made to replace the primary collimator with a silicon crystal.

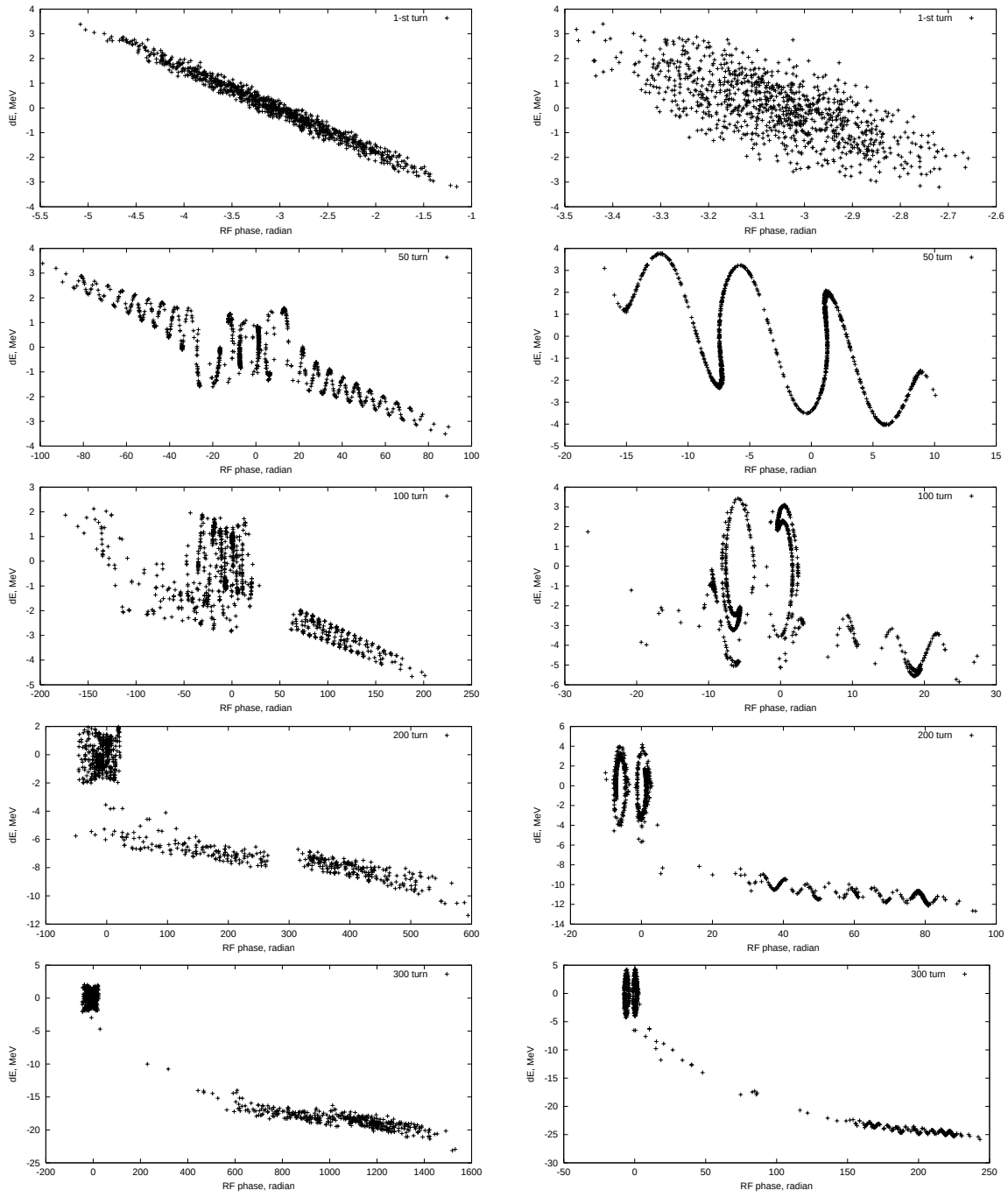

Figure 9.10. Longitudinal phase space at RF capture for f_{RF} = 37.86 MHz (left) and for f_{RF} = 5.41 MHz (right) at the first turn (first line), 50-th turn (second line), 100-th turn (third line), 200-th turn (fourth line), 300-th turn (fifth line). Initial protons are in the vicinity of the unstable point.

The crystal was assumed to have a perfect lattice and crystal surface, with a 1 μm thick amorphous layer on the beam-side of the crystal. The horizontal beam half-size at the crystal is 34.1 mm. The beam amplitude can grow fast due to the space charge effects. We assumed

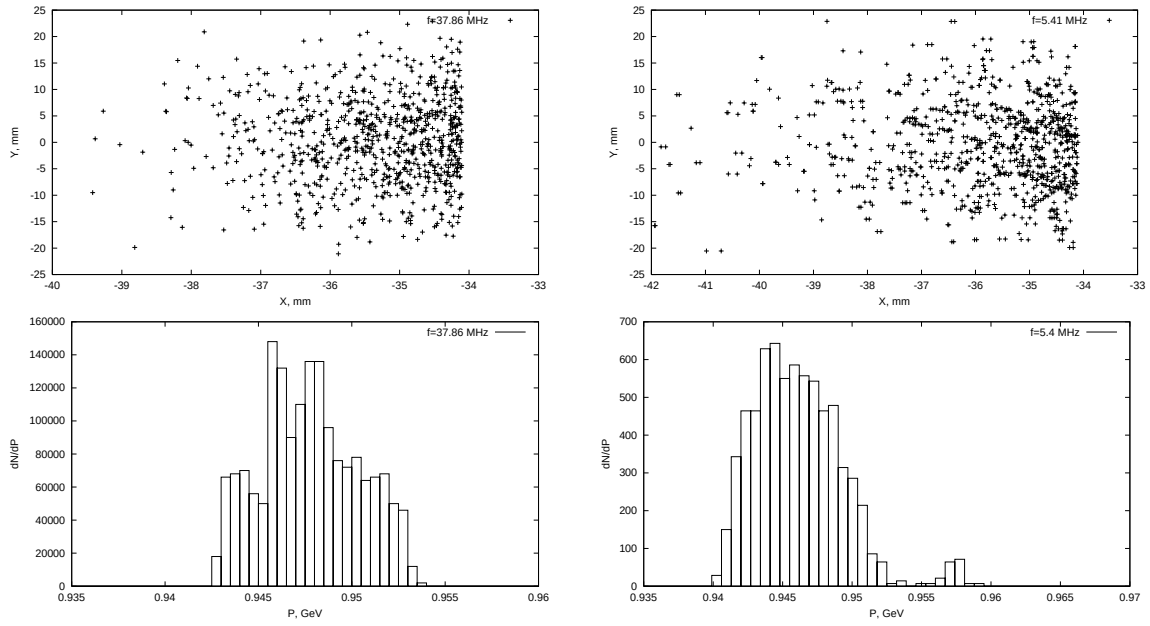

Figure 9.11. Transverse distributions (top) of halo protons on the primary collimator and momentum spectrum of lost protons (bottom) during the RF capture for f_{RF} = 37.86 MHz (left) and for f_{RF} = 5.41 MHz (right).

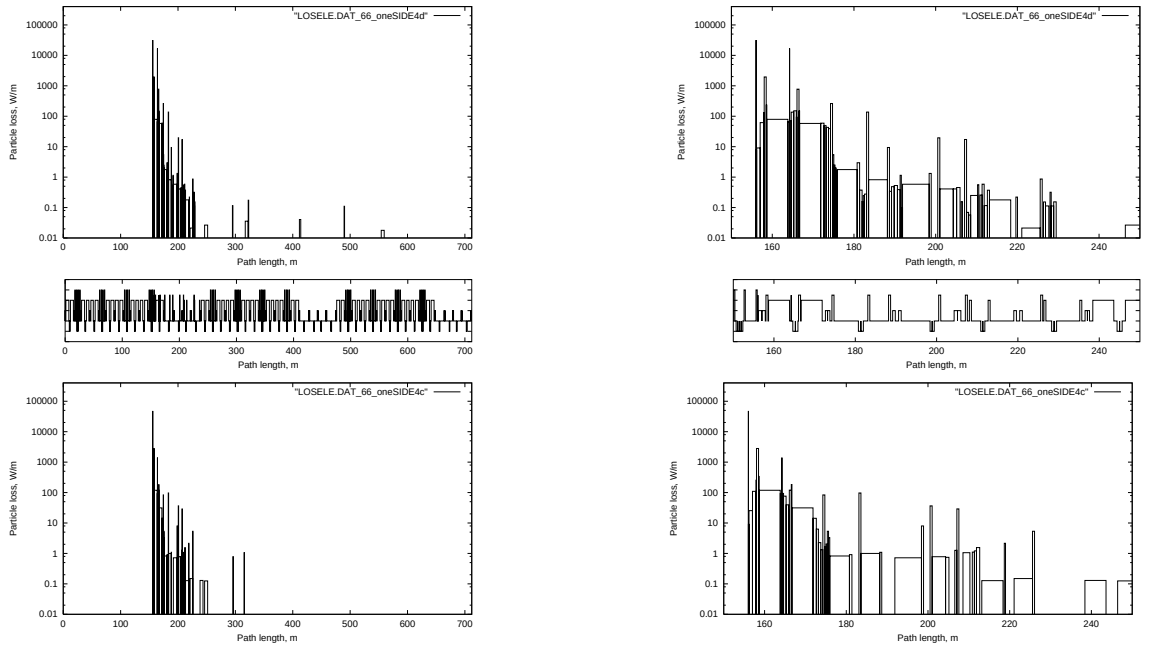

Figure 9.12. Beam losses at injection in the entire ring (left) and in the utility section (right) for the beam size growing slowly with step size of 20 μm (top) and at the RF capture loss (f_{RF} = 37.86 MHz) with a step size of about 2 mm (bottom).

a proton impact parameter at the crystal of 28 μm independent of the beam energy. Then the corresponding beam divergence at the crystal entrance (Fig. 9.13) is ±70 μrad.

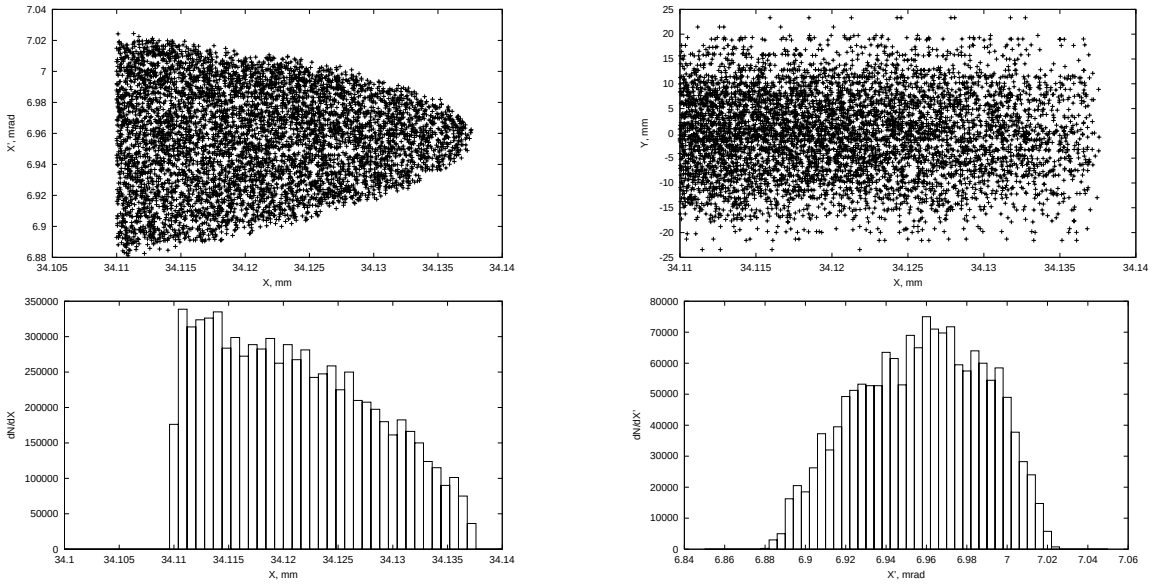

Figure 9.13. Horizontal phase space (top, left), transverse (top, right), horizontal (bottom, left) and angular (bottom, right) distributions of particles at the crystal entrance.

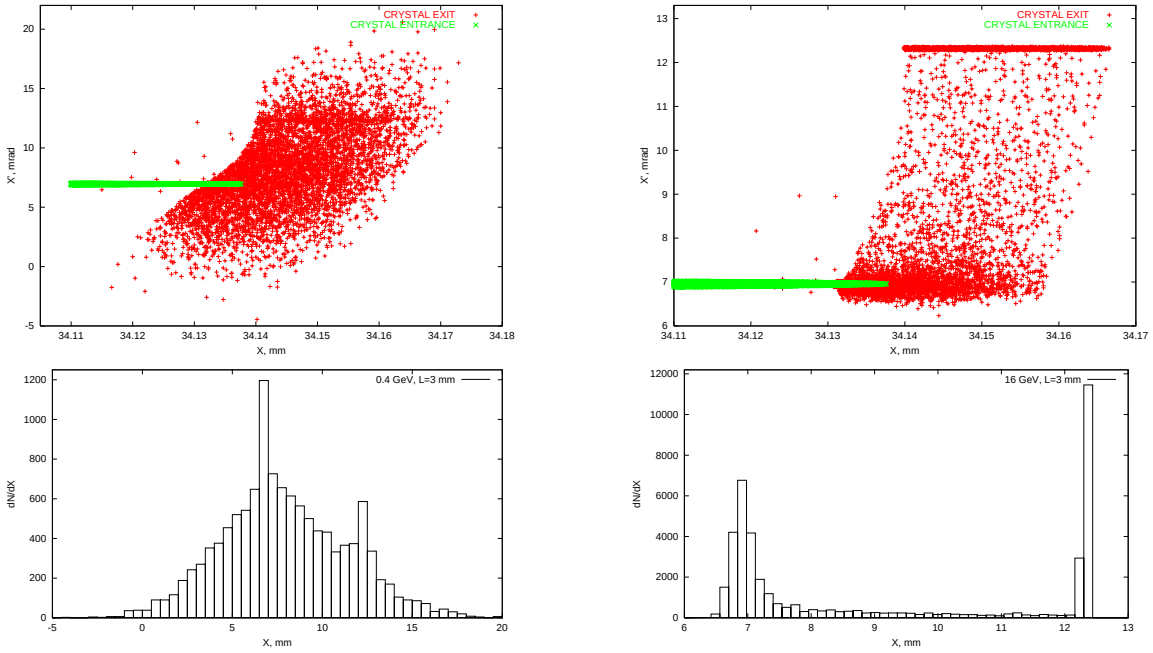

Figure 9.14. Horizontal phase space at a 3-mm crystal entrance and exit (top), and angular distribution at the crystal exit (bottom) at injection (left) and at the top energy (right).

Beam distributions upstream and immediately downstream of a 3 mm silicon crystal are shown in Fig. 9.14. With this crystal L ¡ L_{dechan} at the top energy, but the beam divergence exceeds the critical angle. Therefore, the channeling efficiency at the first pass is only 15%. At injection - although a critical angle (180 μrad) is a factor of 2.6 higher compared to the beam divergence - the efficiency is even lower (5%), because of a very short dechanneling

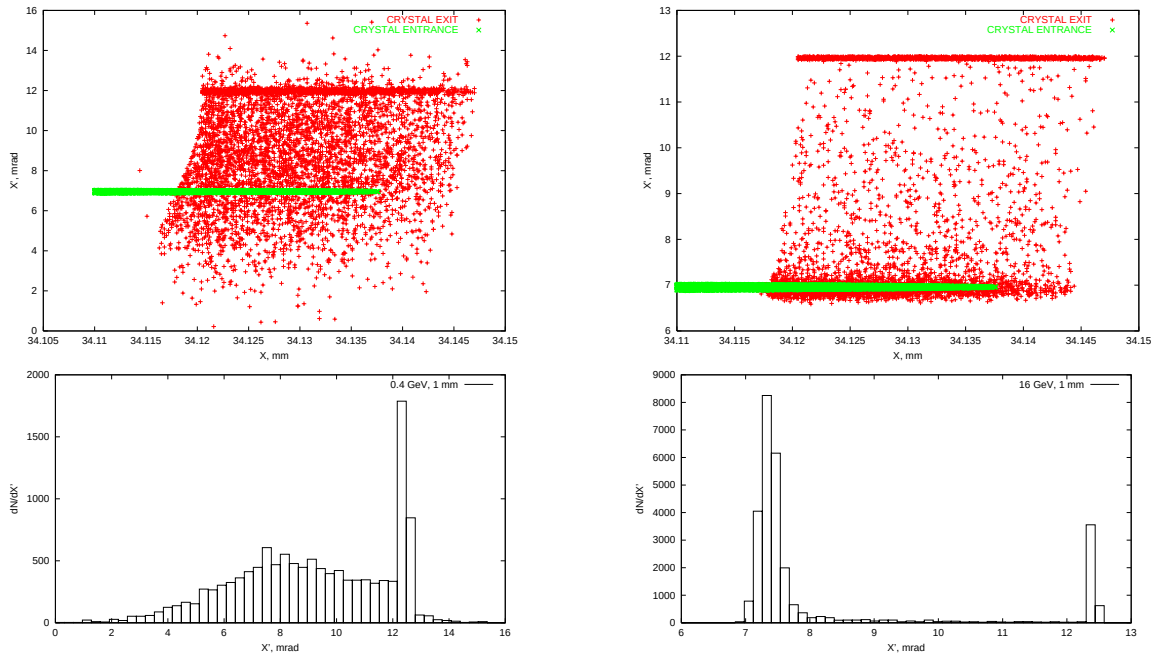

Figure 9.15. Horizontal phase space at a 1-mm crystal entrance and exit (top) and angular distribution at the crystal exit (bottom) at injection (left) and at the top energy (right).

length.

Current technologies allow bending a 1-mm crystal by 1-2 mrad, with a hope to increase this angle to 5 mrad in the near future. This would reduce dechanneling and nuclear interactions in the crystal resulting in a higher channeling/collimation efficiency. We have tried such a crystal in our simulations. Fig. 9.15 gives beam distributions with a 1-mm silicon crystal bent by 5 mrad. Calculated channeling efficiency on the first pass is 15% at the top energy and 21% at injection. A factor of four increase at injection is encouraging. Unfortunately, at the top energy, many protons are not channeled by a short crystal (see Fig. 9.15).

Beam loss rates with such a crystal are compared in Fig. 9.16 and Table 9.6 with those using an amorphous primary collimator. The particle energy loss and multiple Coulomb scattering angle at injection in the 1 mm thick tungsten collimator are quite large (θ_{mcs} = 8 mrad) compared to the dechanneling angle in the silicon crystal (Fig. 9.15). Therefore the losses with the crystal are lower in the main secondary collimators, but they are higher in the supplementary collimators compared to the case with an amorphous tungsten primary collimator. At the top energy, a long tail of dechanneled particles results in about a factor of four higher losses in the utility section at crystal collimation.

Radiation damage to the crystal will limit its use in high-intensity beams. At high dose, the irradiated layers become amorphous. An experiment at the CERN SPS at 450 GeV has shown crystal efficiency reduction by 6% at 10^{18} particles per mm^2 [12, 13]. A limiting flux with the 800 GeV beam at Fermilab was found to be 10^{19} particles per mm^2 [14]. At lower energy the crystal is less sensitive to crystal lattice damage with an acceptable angu-

Table 9.6. Beam loss in the Proton Driver at collimation with a channeling crystal.

	Beam loss		
Collimation system	Utility section	Rest of the ring	Peak loss rate in the ring
	kW	kW	W/m
at the top energy, three supplementary - one-side, two others two-side			
with 3 mm channeling crystal three secondary at 2, 2 and 3 mm five supplementary at 5 mm	11.514	0.006	2.7
with 1 mm channeling crystal three secondary at 2, 2 and 3 mm five supplementary at 5 mm	11.520	0.000	0.0
with primary collimators three secondary at 2, 2 and 3 mm five supplementary at 5 mm	11.497	0.023	2.1
at the injection, three supplementary - one-side, two others two-side			
with 3 mm channeling crystal three secondary at 2, 2 and 3 mm five supplementary at 5 mm	2.879	0.001	0.8
with 1 mm channeling crystal three secondary at 2, 2 and 3 mm five supplementary at 5 mm	2.878	0.002	3.2
with primary collimators three secondary at 2, 2 and 3 mm five supplementary at 5 mm	2.880	0.000	0.0

lar distortion changing as $1/\sqrt{p\beta}$ [13]. Assuming a step size due to a space charge effect of 0.1 mm/turn, one gets a beam size on the crystal of 20 mm$\times$0.1 mm. The proton flux through the crystal is then 10^{17} p/mm^2/hr at 3.3×10^{12} protons lost per accelerator cycle. Assuming radiation hardness of the crystal at 16 GeV of 7×10^{19}p/mm^2, the crystal lifetime is estimated as 800 hours. In a rapid cycling machine RF capture loss can be the main component to be collimated. Step size in this process is of the order of few mm/turn. With that, the proton flux through the crystal is $5\cdot10^{15}$ p/mm^2/hr. This gives 1.5 years for the crystal lifetime.

9.5. Sensitivity Analysis

Optimally aligned primary collimators are placed at the beam edge. The secondary and supplementary collimators are positioned with a small offset with respect to the primary ones. This provides beam halo interaction with primary collimators before interacting with secondary ones. Closed orbit deviation during the cycle and from cycle to cycle can change these conditions if a secondary collimator offset is too small. In a worst case, once the closed orbit has no displacement at the primary collimators, but displacement at the secondary and supplementary ones is large, beam can interact first with the secondary collimators. This

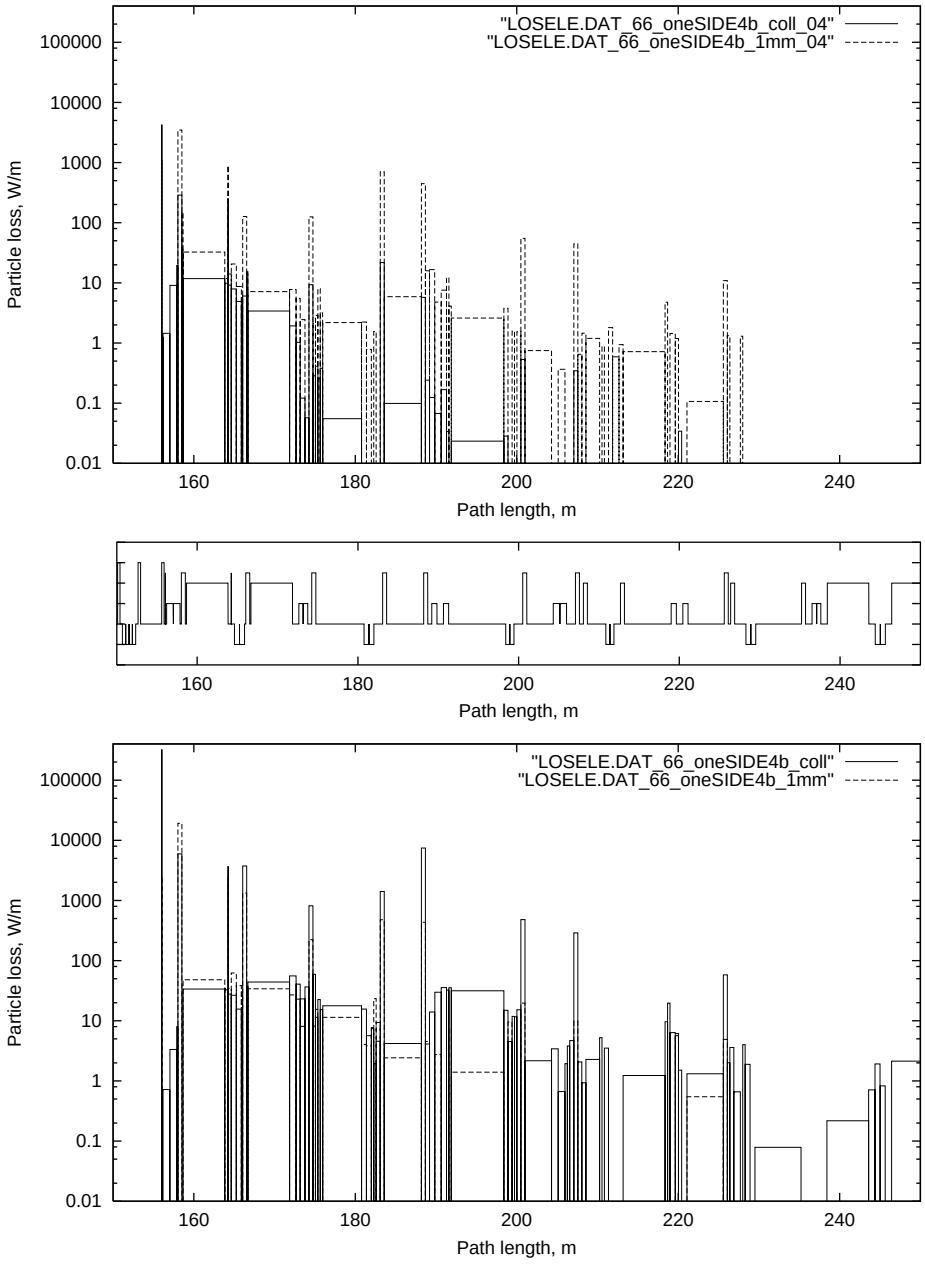

Figure 9.16. Beam loss in the utility section at injection (top) and at the top energy (bottom) for the systems with a 1-mm tungsten primary collimator (solid line) and with a 1 mm silicon crystal (dashed line).

can cause collimator overheating and efficiency degradation. As shown in Table 9.7, positioning of the secondary collimators farther from the beam by 2 mm (from 1 mm to 3 mm) causes beam loss to increase in the ring by 13%, but this allows closed orbit deviation at the locations of collimators up to ± 3 mm without additional heating of secondary collimators.

In our simulations two types of closed orbit are used (Fig. 9.18): (A) closed orbit has

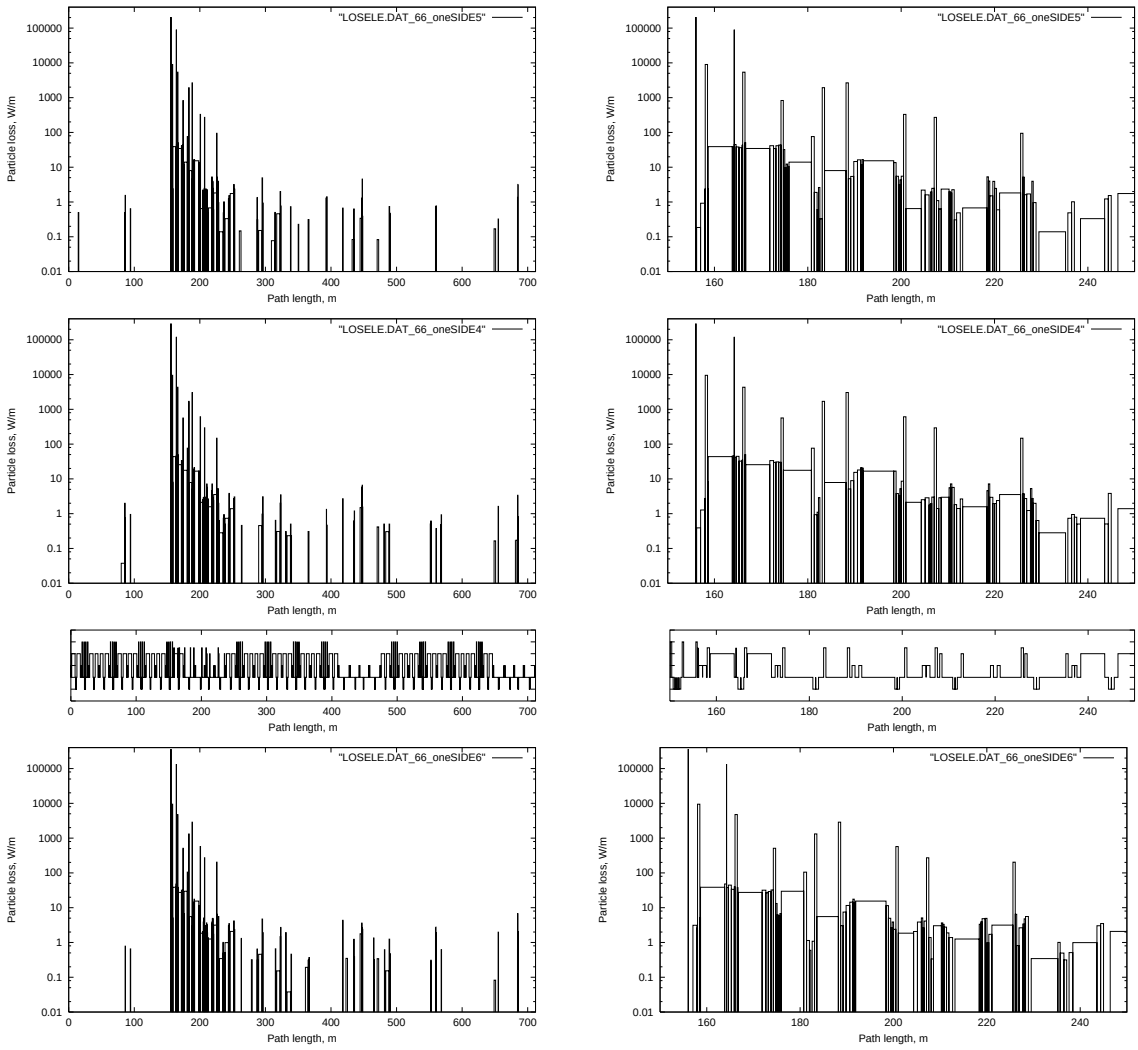

Figure 9.17. Beam loss at the top accelerator energy with 3 secondary and 5 supplementary collimators. Top: secondary collimators are at 1 mm offset and supplementary at 3 mm offset with respect to the primary ones. Middle: secondary are at 2 mm and supplementary at 5 mm. Bottom: secondary at 3 mm and supplementary at 7 mm.

maximum in the primary collimators, and (B) closed orbit has maximum in the secondary and supplementary collimators, and zero in the primary ones. Variations of both orbits were done in the range of ± 4 mm. Beam loss distributions for different closed orbit configurations in the system with secondary collimators at 2 mm, and supplementary ones at 5 mm from the beam are presented in Table 9.8. At orbit deviation of ± 4 mm, the number of protons lost outside the collimation region increases from 0.4% to 1.5% and peak loss in the ring from 5 W/m to 50 W/m.

The betatron tune deviation causes a change of phase advance between collimators and the distance to the resonances. As the betatron amplitude of protons after interaction with the primary collimator is large, the second factor can degrade collimation efficiency. Beam

Table 9.7. Beam loss at the top energy for different positions of secondary collimators with respect to the beam.

Collimators	Beam loss		
collimation system	Utility section	Rest of the ring	Peak loss rate in the ring
	kW	kW	W/m
primary three secondary at 1 mm five supplementary at 3 mm	11.497	0.023	9.5
primary three secondary at 2 mm five supplementary at 5 mm	11.469	0.050	5.4
primary three secondary at 3 mm five supplementary at 6 mm	11.457	0.062	10.6

losses in the machine at the top energy as a function of accelerator tune are presented in Table 9.9. Accelerator tune deviation mostly affects the value of peak loss in the machine.

Table 9.8. Beam loss at the top energy as a function of closed orbit deviation.

	Beam loss		
Maximum closed orbit deviation	Utility section	Rest of the ring	Peak loss rate in the ring
mm	kW	kW	W/m
closed orbit type A			
-4	11.442	0.078	19.2
-3	11.454	0.066	18.1
-2	11.465	0.055	12.3
-1	11.461	0.059	14.0
0	11.470	0.050	5.4
1	11.463	0.053	12.5
2	11.452	0.065	11.4
3	11.448	0.072	9.4
4	11.398	0.122	26.8
closed orbit type B			
-4	11.348	0.172	49.6
-2	11.436	0.084	14.8
0	11.470	0.050	5.4
2	11.454	0.066	10.9
4	11.466	0.054	16.7

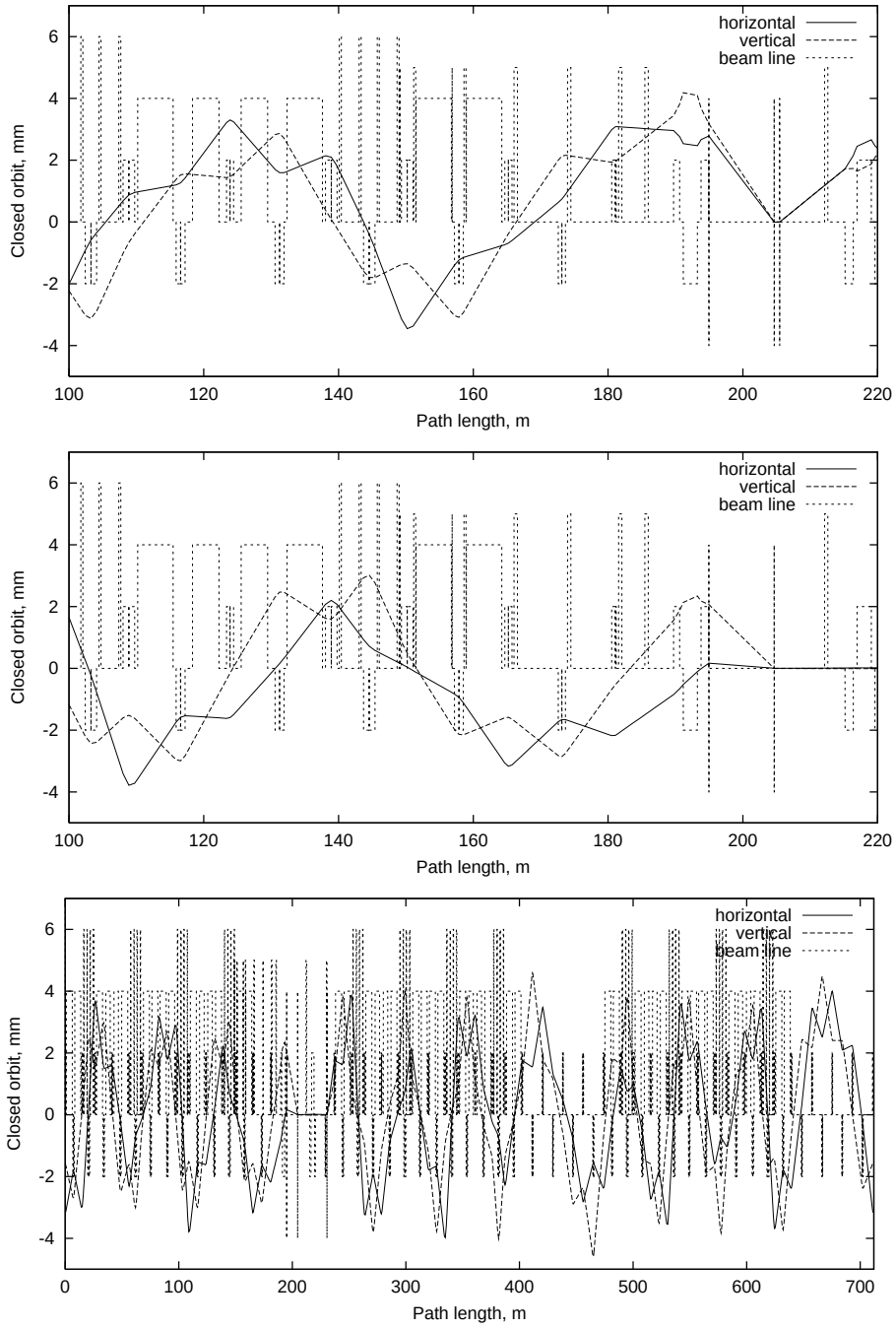

Figure 9.18. Closed orbit deviations at collimation system sensitivity analysis. Top: type A - orbit with maximum deviation in the primary collimators of -3 mm, middle and bottom: type B - orbit with zero deviations in the horizontal primary collimator.

9.6. Beam Accident

Consider a consequence to the machine components of an uncontrolled loss of a single pulse at 16 GeV for 3×10^{13} protons in Phase-I (1.2 MW) and 1×10^{14} protons in Phase-II (4 MW).

Table 9.9. Beam loss at the top energy as a function of accelerator tune.

	Beam loss		
tune	Utility section	Rest of the ring	Peak loss rate in the ring
	kW	kW	W/m
$\nu_x = 11.443,\ \nu_y = 11.351$	11.473	0.047	134.7
$\nu_x = 11.431,\ \nu_y = 11.369$	11.460	0.060	14.9
$\nu_x = 11.407,\ \nu_y = 11.407$	11.463	0.057	127.7
$\nu_x = 11.378,\ \nu_y = 11.416$	11.477	0.043	14.5
$\nu_x = 11.363,\ \nu_y = 11.421$	11.484	0.036	14.5

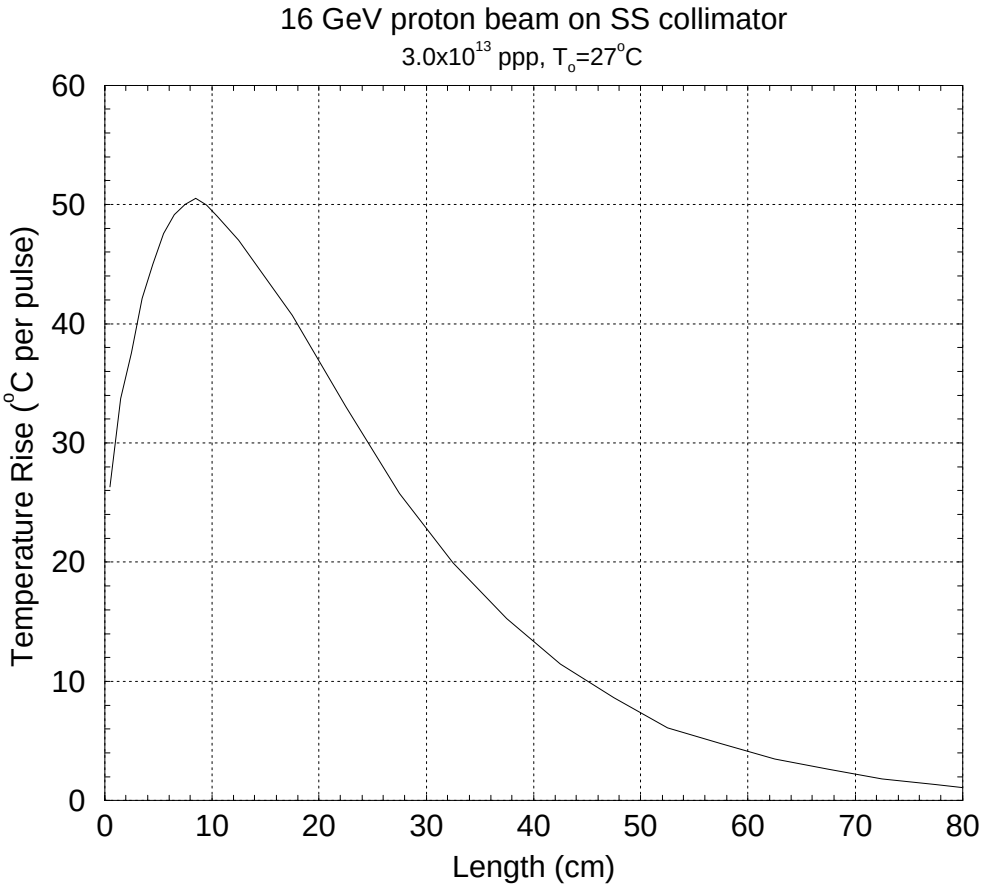

Figure 9.19. Instantaneous temperature rise in a secondary collimator jaw at beam axis *versus* jaw length.

A beam after painting is assumed to have a quasi-rectangular shape of a 7×5 mm half-size. This beam hits a beam pipe at a grazing angle or a jaw of a secondary collimator. Initial

temperature is assumed to be 27°*C*. Hadronic and electromagnetic showers are calculated with MARS14.

9.6.1. Beam pipe

Elliptical beam pipe dimensions are 5×9 inches with stainless steel walls 0.127 or 1.27 mm thick. Beam grazing angles are α=2, 5 and 10 mrad. Depending on the β-function, the maximum instantaneous temperature rise ranges from 33 to 38.5°*C* for a 0.127-mm beam pipe and from 41 to 48°*C* for a 1.27-mm beam pipe for the Phase-I beam. With Phase-II parameters, these numbers are roughly three times higher, but still quite acceptable. An accidental loss of successing pulses on a beam pipe exactly at the same location is unlikely; therefore one can conclude that this is not problem.

9.6.2. Collimator jaws

If a single 16-GeV pulse of 3×10^{13} protons hits normally at the center of a 3 cm thick and 80 cm long stainless steel or copper jaw of a secondary collimator, Fig. 9.19 shows the instantaneous temperature rise in the jaw immediately after the pulse at the beam axis as a function of the jaw length. One sees that ΔT_{max}=50°*C*. With Phase-II parameters, this value is roughly three times higher. This is still quite acceptable. With an appropriate cooling system, several such pulses on the same collimator could be allowed.

9.7. Collimators

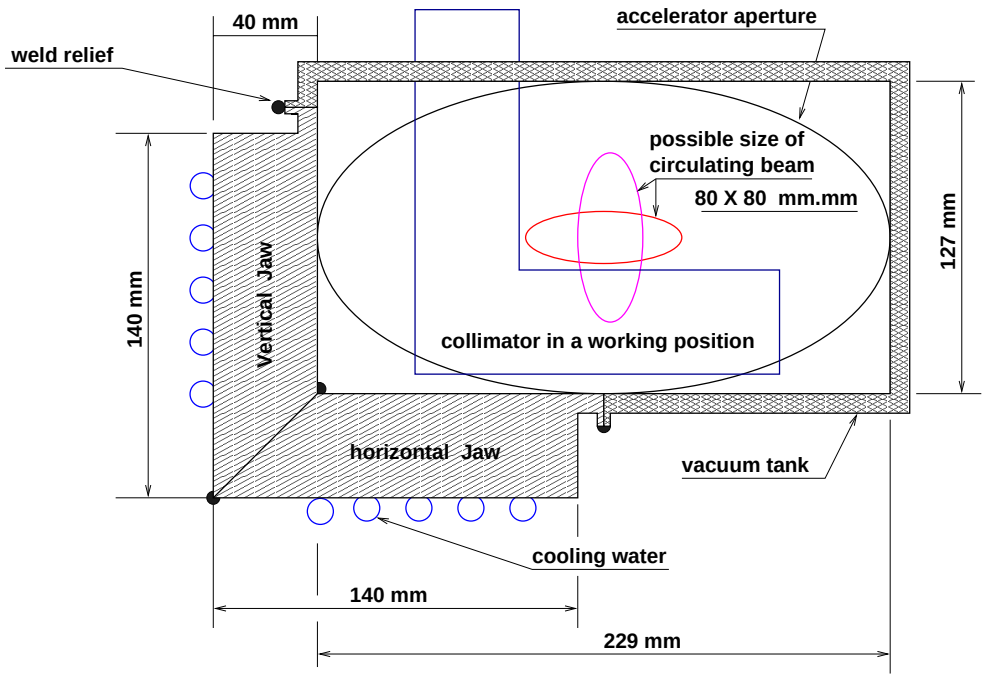

Figure 9.20. Secondary collimator cross section.

9.7.1. Requirements

The secondary collimators are chosen to be L-shaped stainless steel with L_x = 140 mm, L_y = 140 mm, thickness=40 mm, and length = 500 mm (Fig. 9.20). The primary collimators are chosen to be one-side jaw, tungsten with L_x = 140 mm, L_y = 140 mm, thickness=30 mm, and length=1 mm. These dimensions will accommodate the full beam size, after painting, and will accommodate maximum impact parameters. All collimators will be in a fixed position during the machine cycle, but motion control is required in order to adjust collimators to their optimum position.

9.7.2. Mechanical design

The mechanical design of the collimators and targets will be similar to those already built and installed in the Tevatron for Collider Run II [15, 16, 17]. Those collimators consist of 2 pieces of stainless steel, 0.5 m long, welded together in an "L" configuration. Machining and assembly tolerances of 25 μm are easily met for the collimator steel. The collimator assembly is welded inside a stainless steel box of outside dimensions approximately 230 mm x 130 mm and with bellows on each end. The box assembly is supported by a cradle which is moved independently in the vertical and horizontal directions by stepping motors. Full range of motion is 50 mm in steps as small as 25 μm if required and a maximum speed of 2.5 mm/sec. The collimator speed can be increased if a larger minimum step size is acceptable. Position readback is provided by linear differential voltage transformers, although investigation into the radiation hardness of these devices is required. Mechanical damage is prevented by limit switches on all degrees of motion. The entire assembly, including bellows, will occupy approximately 1 m of lattice space. The target assembly is identical to the collimator assembly except that the target "L" blocks are only 0.1 m in length. The 1 mm thick machined tungsten targets are bolted to the stainless steel blocks. The blocks provide a good heat sink for energy dissipated in the tungsten. The entire assembly, including bellows, will occupy approximately 0.6 m of lattice space.

9.7.3. Controls

The motion controls for the collimators will be similar to the system already installed for the Tevatron Collider Run II collimators [15, 16], but without local loss monitor feedback. This system is also currently in use with other movable devices in the Fermilab accelerator complex. Up to 4 motors and 4 position readbacks will be controlled and monitored by a single MVME162 processor running VXWORKS in a VME crate in a nearby service building. Stepping motors and LVDT's are interfaced to the CPU via commercial IP's (Industrial Packs). The motor PS and motor controllers are also commercial hardware. A total of 3 "stations" – VME crate, motor controller crate, and motor PS will be required for the entire system of 10 collimators.

9.7.4. Cooling

A total of 11.5 kW of DC power is expected to be dissipated in the collimators. 11.5 kW of power can be removed from a single collimator by circulating standard LCW (Low Conductivity Water) through cooling channels on the outside of the collimator box. A flow of 2.2 gpm will remove 11.5 kW of power with a temperature rise of 20C. The requirement is that there is good thermal contact between the stainless steel "L" blocks and the welded box.

9.8. Conclusions

Detailed energy deposition studies performed in the machine elements give the tolerable beam loss in the Proton Driver. At the top energy in the arc for the proposed lattice, hands-on maintenance limits are 0.25 W/m in the open long beam pipes and 3 W/m in the magnets, while the ground-water limit is 1 W/m.

A 3-stage collimation system has been proposed based on detailed Monte-Carlo simulations at injection, top energy and at RF capture. The system consists of 1-mm thick tungsten primary collimators positioned at the horizontal and vertical edges of the beam after painting, followed by three secondary collimators with 2 mm offset with respect to the primary collimators and five supplementary collimators at 5 mm from the beam edge. Secondary and supplementary 0.5 m long stainless steel collimators are aligned with respect to the beam envelope after painting. Such a system allows localization of more than 99% of beam loss in a special 80 m long utility section. Beam loss in the rest of the machine is on average 0.2 W/m. Crystal collimation appears to not be efficient in the Proton Driver because of the large divergence of halo distribution at the crystal entrance. Local shielding proposed in the hottest 30-m part of the utility section is described in Chapter 10. Overall, despite challenging parameters of the proposed new Proton Driver, beam loss and induced radiation effects can be controlled and reduced to allowable levels.

References

[1] A. I. Drozhdin, O. E. Krivosheev and N. V. Mokhov, "Beam Loss, Collimation and Shielding at the Fermilab Proton Driver", Fermilab-FN-693 (2000).

[2] O. E. Krivosheev and N. V. Mokhov, "Tolerable Beam Losses and Shielding", *Proc. of the 7th ICFA Mini-Workshop on High-Intensity, High-Brightness Hadron Beams "Beam Halo and Scraping"*, September 13-15, 1999, Lake Como, Wisconsin.

[3] A. I. Drozhdin, C. J. Johnstone and N. V. Mokhov, "16 GeV Proton Driver Beam Collimation System", *Proc. of the 7th ICFA Mini-Workshop on High-Intensity, High-Brightness Hadron Beams "Beam Halo and Scraping"*, September 13-15, 1999, Lake Como, Wisconsin.

[4] I. S. Baishev, A. I. Drozhdin and N. V. Mokhov, "STRUCT Program User's Reference Manual", SSCL–MAN–0034 (1994); http://www-ap.fnal.gov/∼drozhdin/.

[5] N. V. Mokhov, "The MARS Code System User's Guide", Fermilab-FN-628 (1995); N. V. Mokhov, S. I. Striganov, A. Van Ginneken, S. G. Mashnik, A. J. Sierk, and J. Ranft, "MARS Code Developments", Fermilab-Conf-98/379 (1998); N. V. Mokhov, "MARS Code Developments, Benchmarking and Applications", Fermilab-Conf-00/066 (2000). N. V. Mokhov and O. E. Krivosheev, "MARS Code Status", Fermilab-Conf-00/181 (2000). http://www-ap.fnal.gov/MARS/.

[6] A. I. Drozhdin and O. E. Krivosheev, "The Fermilab Proton Driver Beam Injection System Simulations", Fermilab–FN–694 (2000).

[7] "The NuMI Facility Technical Design Report", Fermilab (1998).

[8] A. I. Drozhdin, N. V. Mokhov et al., SSCL-Preprint-555 (1994).

[9] D. A. Edwards and M. J. Syphers, "An Introduction to the Physics of High Energy Accelerators", Wiley Series in Beam Physics and Accelerator Technology (1993).

[10] V. M. Biryukov, A. I. Drozhdin and N. V. Mokhov, "On Possible Use of Bent Crystal to Improve Tevatron Beam Scraping", *Proc. of the 1999 Particle Accelerator Conference*, New York, New York, March 29 - April 2, 1999, pp. 1234-1236; also Fermilab-Conf-99/072 (1999).

[11] V. M. Biryukov, "Crystal Channeling Simulation - CATCH 1.4 User's Guide", CERN SL/Note 93-74(AP) (1993).

[12] V. M. Biryukov, Yu. A. Chesnokov and V. I. Kotov, "Crystal Channeling and its Application at High Energy Accelerators", Berlin: Springer (1997).

[13] V. M. Biryukov, Private communication, IHEP (1999).

[14] C. T. Murphy, Private communication, Fermilab (1999).

[15] M. Church, "Proposed Tevatron Collimation System for Collider Run II", International Symposium on Near Beam Physics, ed. R Carrigan and N Mokhov, Fermilab, Batavia, IL, p. 134 (1997)

[16] M. Church, "Update on the Tevatron Collimator System for Collider Run II", in 7th ICFA Mini-Workshop on Beam Halo and Scraping, ed. W Chou and N Mokhov, Lake Como, WI, (1999)

[17] R. Reilly, Fermilab Assembly Drawing 1720.004-ME-326216 Rev. A (1998)